Flux-lattice melting and flux creep in a high-T_c superconductor

1989 J. Phys.: Condens. Matter 1 8945

(http://iopscience.iop.org/0953-8984/1/45/018)

J. Phys.: Condens. Matter **1** (1989) 8945–8960. Printed in the UK

Flux-lattice melting and flux creep in a high-T_c superconductor

R S Markiewicz† §‖, K Chen†‖, B Maheswaran†‖, A G Swanson‡ and J S Brooks‡

† Physics Department, Northeastern University, Boston, MA 02115, USA

‡ Physics Department, Boston University, Boston, MA 02215, USA

Received 11 November 1988, in final form 24 February 1989

Abstract. We report measurements of the magnetisation-derived critical current j_c in $TlBa_2Ca_3Cu_4O_x$, a 122 K superconductor. Analysis of the field H^*_{c2}, at which j_c scales to zero, naturally falls into two regimes: a low-temperature regime, which can be described by flux-lattice melting, and a high-temperature regime dominated by flux creep. In the latter regime, the scaling of both H^*_{c2} and the sample resistivity with temperature are in good agreement with a model proposed by Tinkham, when anisotropy effects are taken into account. From the former regime, we infer $H_{c2\|}(T = 0) \simeq 430$ T.

1. Introduction

For high-critical-current (j_c) applications of the new high-T_c oxide superconductors [1], the effects of pinning must be studied in detail. In these studies, analysis of the scaling properties of the bulk pinning force $F_p = j_c H$, where H is the applied magnetic field, has proven extremely valuable. Recently, it has been shown [2, 3] that the new high-T_c superconductors obey a simple scaling law similar to the form proposed by Kramer [4]:

$$F_p = \gamma^2 H_c^2 H^{1/2}(1 - b)^2 \tag{1}$$

where H_c is the thermodynamic critical field, $b = H/H^*_{c2}$, and γ is a constant $\simeq 1700$, if j_c is in A cm^{-2} and all fields are in T. However, in Kramer's theory, $H^*_{c2} = H_{c2}$, the upper critical field, whereas most high-T_c experiments show $H^*_{c2} < H_{c2}$. The experiments measure either the transport critical current in a thin film [2] or the magnetisation critical current in a bulk polycrystalline pellet [3]. The present paper reports both magnetisation and magnetoresistance measurements on a new material, a four-copper-layer Tl-based compound with $T_c = 122$ K. Measurement of the scaling field $H^*_{c2}(T)$ allows reconstruction of a flux lattice H–T phase diagram. Three phases are found: a flux lattice, a fluid and a 'glassy' phase. The boundary between fluid and glassy phases may be purely kinetic, determined by the point at which flux-lattice motion becomes negligible on the experimental timescale. This boundary is in good agreement with a scaling form

§ Also at: Department of Physics, Boston University, Boston, MA 02215, USA.

‖ Also at: Barnett Institute, Northeastern University, Boston, MA 02115, USA.

0953-8984/89/458945 + 16 $02.50

proposed by Tinkham [5], based on a thermal activation model of Yeshurun and Malozemoff [6] (YM). The lattice melting transition appears to be in agreement with theoretical predictions, if allowance is made for pinning effects.

2. Experimental details

The material used is a four-copper-layer Tl oxide [7], with the ideal (stoichiometric) formula $TlBa_2Ca_3Cu_4O_x$ (1234). From a starting material of composition $TlPb_{0.25}BaCa_4Cu_4O_x$, a yield of ~80% of the 1234 material was achieved, with the remainder predominantly a (non-superconducting) cubic perovskite. The critical temperature scales with number of Cu layers, and for this four-layer compound $T_c = 122$ K (figure 1). Two forms of sample are used: either pressed, sintered pellets, or field-oriented

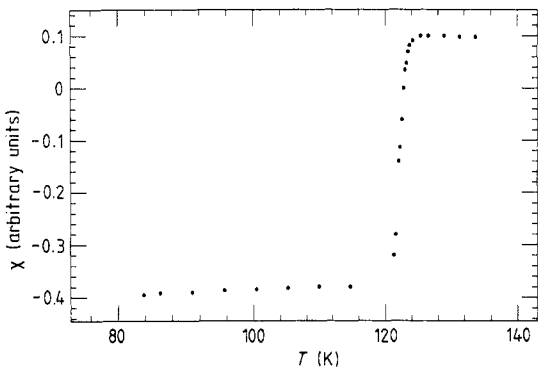

Figure 1. AC susceptibility χ of $TlBa_2Ca_3Cu_4O_x$, showing sharp drop at $T_c = 122$ K.

grains [3, 8] dispersed in epoxy. The degree of orientation P is defined from x-ray reflection intensities. While it is a convenient measure of relative orientation, some care must be exercised in interpreting its value. Thus the present value $P = 98\%$ still corresponds to a 10^0 gaussian spread in the c axis. The precise definition is discussed in appendix 1.

Two kinds of experiment were performed: the magnetoresistance of the pressed pellets was measured in fields up to 15 T, from 77–250 K; also, the magnetisation j_c was determined for both types of sample, following standard procedures. A hysteresis loop of magnetisation against field was measured at a series of different temperatures. From the width of the hysteresis loop, ΔM, the critical current was determined using the critical-state model [9]

$$\Delta M = rj_c/\alpha \tag{2}$$

where r is a typical grain radius ($r \sim 5\mu$m) and $\alpha = 17$ for a spherical grain. Note that, because of the unusual weak-link behaviour of the high-T_c superconductors, it is the

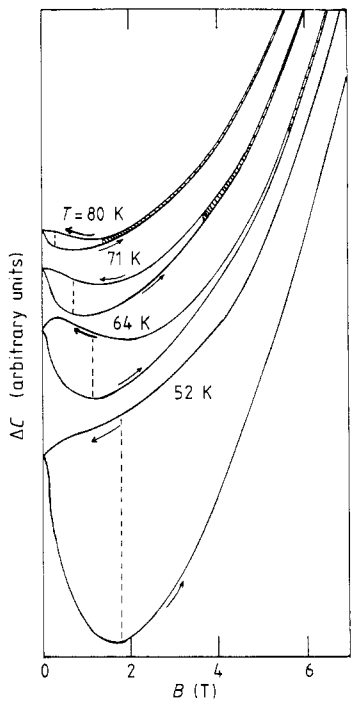

Figure 2. Capacitance $\Delta C \propto MH$, for unoriented polycrystalline pellet, showing H_m (broken lines) and H^*_{c2} (region above H^*_{c2} is hatched).

individual grain radius r that enters equation (2) rather than the total sample radius. This is because the external field readily breaks down the weak Josephson connections between grains, so that the magnetisation hysteresis is a measure of *intragrain* j_c. The weak Josephson links also act to suppress the transport j_c, which is typically orders of magnitude smaller than the magnetisation j_c in a polycrystalline sample.

Magnetisation measurements on the epoxy sample were carried out using a commercial SQUID magnetometer, with fields of up to 5 T aligned either parallel or perpendicular to the c axis (low-conductivity direction). Measurements on the pressed pellet were made using a capacitance magnetometer [10], which allowed operation up to 15 T, with simultaneous measurement of sample resistivity. The SQUID data were accumulated at a slow rate, taking ~40 min per point to allow the field to stabilise. By contrast, the full-capacitance data could be accumulated in 2 min, although 10 min was more typical

3. Results

Figure 2 shows typical data for the hysteretic magnetisation of a pressed, unoriented pellet of the Tl superconductor, taken using the capacitance magnetometer. The output is ΔC, the change of the capacitance in a magnetic field due to a force or torque acting on the sample attached to one (adjustable) plate of the capacitor. The force has the form

$$F_m = M_z \, dB/dz \tag{3}$$

while a torque $\boldsymbol{\tau} = \boldsymbol{M} \times \boldsymbol{B}$ can also lead to a capacitance change. In either case,

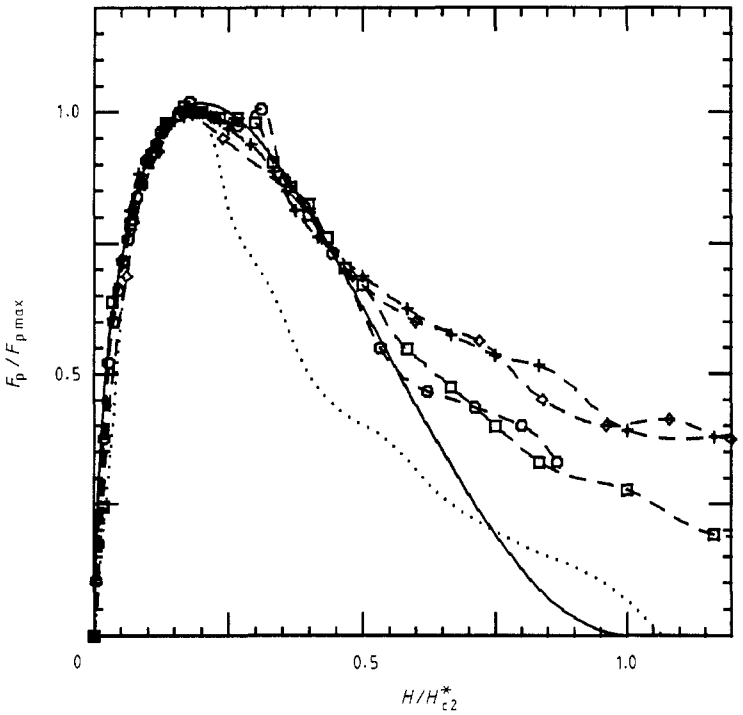

Figure 3. F_p/F_{pmax} against H/H^*_{c2}, for the data of figure 2 (broken curves) against equation (1) (full curve). Dotted curve is that generated with minor hysteresis loops.

$\Delta C \propto MB$, so the width of the hysteresis is directly proportional to F_p. By moving the sample to the centre of the magnet ($dB/dz = 0$) it was found that the torque term is very small in the present configuration. In these experiments, the samples were placed off-centre, so $\Delta C \propto F_m$. The parabolic increase of ΔC at high fields is due to a paramagnetic contribution in the normal state. The vertical broken lines in figure 2 show the maxima of the hysteresis loops, proportional to F_{pmax}, at fields H_m. The magnetisation hysteresis is replotted in scaled form in figure 3, as F_p/F_{pmax} against H/H^*_{c2}, taking $H^*_{c2} = 5H_m$, as given by equation (1). All four data sets follow the same scaling behaviour, which is in basic agreement with equation (1) (full curves).

One problem is evident with the capacitance data in figures 2 and 3: there is a small, residual, nearly-field-independent hysteresis at fields $>H^*_{c2}$. This is not a real magnetisation effect, but varies with sweep rate. By sweeping slowly and looking at minor hysteresis loops, reversing the field about once per tesla, it can be shown that ΔM goes to zero near H^*_{c2}. Unfortunately, the width of the minor hysteresis loops underestimates ΔM. The dotted curve in figure 3 shows a typical scaling curve using these minor loops. Hence, the most accurate way to determine H^*_{c2} is either by taking $H^*_{c2} = 5H_m$, or by replotting the data as in figure 4 (discussed below) and extrapolating the linear region.

Equation (1) can be rewritten

$$j_c^{1/2} H^{1/4} = \gamma H_c (1 - b) \tag{4}$$

showing that a plot of the left-hand side of equation (4) against H will yield a straight line with intercept $H = H^*_{c2}$. Figure 4 shows typical data taken for the same sample as in

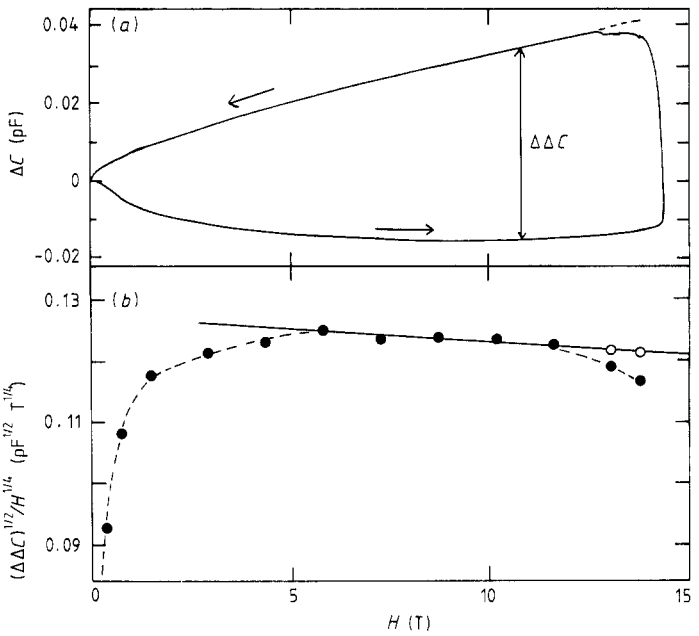

Figure 4. (*a*) Capacitance $\Delta C \propto MH$, at $T = 4.2$ K, for same sample as figure 2. Arrows show direction of field sweep. Note that curve drops below full hysteresis loop (broken curve) due to field reversal near 15 T. (*b*) Scaling of j_c (equation (4)), for the data in (*a*). Open circles correspond to corrected data (broken curve in (*a*)); full line is equation (4); dashed curve is a guide to the eye.

figures 2 and 3, using the capacitance magnetometer, at $T = 4.2$ K. Figure 4(*a*) shows ΔC against field and the capacitance hysteresis, $\Delta\Delta C$, proportional to ΔM. Figure 4(*b*) shows the scaling of the data, after equation (4). Several features should be noted. First, equation (4) must break down at sufficiently low fields, since j_c becomes a field-independent constant, and the left-hand side of equation (4) must go to zero. This is clearly seen in the data for $H < 5$ T. Secondly, when the direction of field sweep is reversed, there is a certain interval of field variation over which the hysteresis is smaller than the Bean model value: compare the full and broken curves of figure 4(*a*) near $H =$ 15 T. This is an expected consequence of following a minor hysteresis loop (i.e. reversing the field sweep direction at a field below H_{c2}), as mentioned in appendix 2. The magnitude of the resulting error can easily be estimated by generating a smaller hysteresis loop (e.g. by reversing the field at 5 T) and seeing how it deviates from the full (to 15 T and back) curve. This is how the broken curve in figure 4(*a*) was generated. The open circles in figure 4(*b*) correspond to the broken curve data of figure 4(*a*). It can be seen that without this correction, the scaling parameter would drop below the straight line at the highest fields. Extrapolating the straight line in figure 4(*b*), j_c scales to zero at 290 T.

Figure 5 shows more extensive data on the scaling (equation (4))(. The data are from a sample mounted in epoxy, taken using the SQUID susceptometer, and hence are limited to fields below 5 T. The linear behaviour of equation (4) is found for H parallel to the a, b plane (figure 5(*a*)) but not for perpendicular to a, b (figure 5(*b*)). At high temperatures, the $j_{c\perp}$ data seem to be a superposition of two linear segments. At low fields, the $j_{c\perp} > j_{c\parallel}$, but $j_{c\perp}$ falls off faster with field. Near the point where the two curves

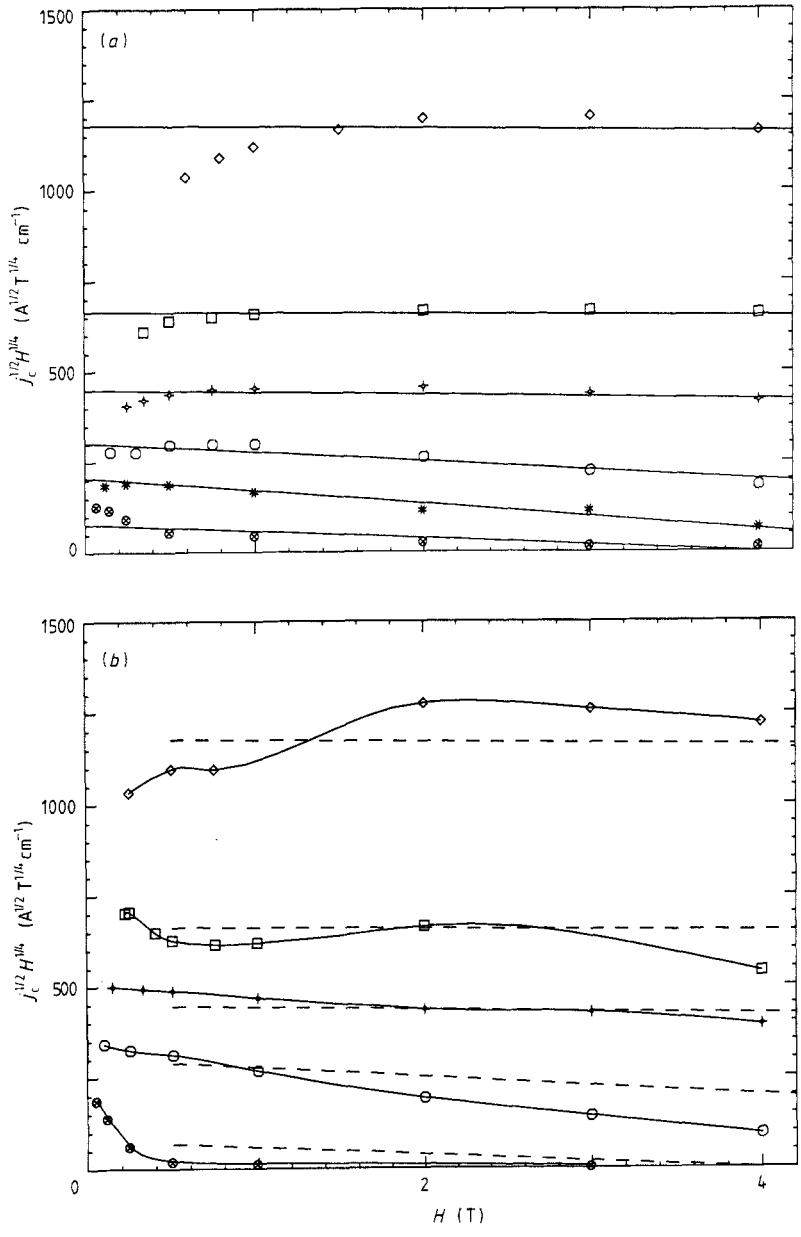

Figure 5. (*a*) Scaling of j_c for H parallel to a, b. Data are at $T = 4$, 15, 25, 40, 55 and 70 K (in order of decreasing j_c). Straight lines are fits to equation (4). (*b*) Similar plots for H perpendicular to a, b. Same symbols as in (*a*). Full curves are guides to the eye; broken lines are high-field $H_\parallel$-behaviour (taken from (*a*)).

cross, the $j_{c\perp}$ scaling curve changes over to another line more nearly parallel to the $j_{c\parallel}$ data (broken lines). At low temperatures, this behaviour is complicated by the presence of a broad peak in the scaling curve. A similar behaviour was found in a lower-T_c Tl compound [3], and a possible explanation will be discussed below. Due to the limited number of data points, the high-field correction discussed above (broken curve in figure

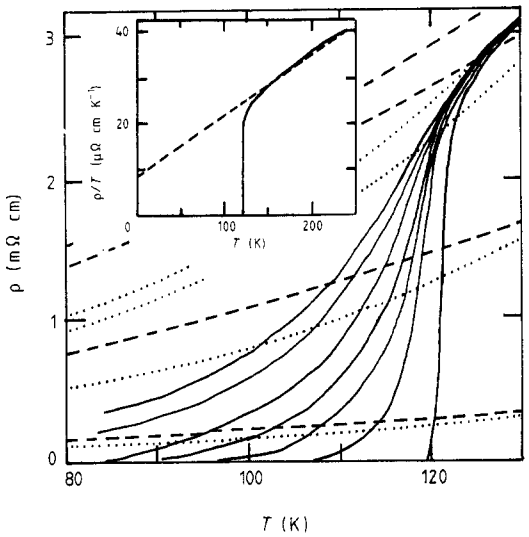

Figure 6. Resistivity against temperature at fields $H = 0, 0.37, 1.5, 3.0, 5.2, 11.1$ and 14.4 T, in order of increasing broadening. Broken curves are extrapolated normal-state resistances ρ_n (equation (5)) and 0.9, 0.5 and 0.1 ρ_n, with ρ_n taken from inset. Dotted curves are the same curves for alternative normal state ρ_n (equation (6)). Inset: ρ/T against T (full curve), with best fit to equation (5) (broken line).

4(*a*)) could not be made. Nevertheless, the scaling results of the two measurements are in good agreement: j_c scales to zero at 260 T at 4 K (figure 5(*a*)), whereas the capacitance magnetometer yielded $H_{c2}^{*} = 290$ T at 4.2 K. At these high fields, the scaling behaviour, even in an unoriented sample (figure 4), will be dominated by the parallel critical field.

Figure 6 shows plots of sample resistance against temperature at a series of magnetic fields. The large broadening of the transition is clearly observed. No net magnetoresistance could be detected in the normal state. While the normal-state resistivity, ρ, varies approximately linearly with T, it has the unusual feature that any straight-line approximation will extrapolate to zero at a $T \gg 0$. We have been able to fit the full curve to the form

$$\rho = A_1 T + A_2 T^2 \tag{5}$$

where A_1 and A_2 are constants: $A_1 = 8.5\ \mu\Omega$ cm K^{-1}, $A_2 = 0.12\ \mu\Omega$ cm K^{-2}. The inset in figure 6 shows a plot of ρ/T against T. Systematic deviations from linear behaviour suggest that the non-linear power may be slightly less than two. Note that in a field, ρ decreases smoothly to zero as T decreases, and it is very difficult to estimate the threshold field, H_{c2}^{T}, at which resistance first appears. This threshold apears to be somewhat sharper in plots of ρ against H at fixed T (figure 7). These measurements were made simultaneously on two samples, one fresh (less than 1 week old), the other aged for about two months. The results were virtually identical, showing that ageing is not a severe problem with these materials.

In comparing ρ with theory, we would ideally like to plot level curves, $H(\delta)$ against T, where $\delta = \rho/\rho_n$ is a fixed ratio of ρ to its normal-state value. This, however, requires extrapolation of ρ_n to $T < T_c$. Use of equation (5) is questionable since, as seen in the inset to figure 6, ρ/T deviates from linear behaviour for $T < 150$ K. This behaviour has been observed in other high-T_c superconductors, and is usually interpreted as a fluctuation effect (although the field dependence is surprisingly weak). The broken curves in figure 6 show level curves based on equation (5), for $\delta = 1.0, 0.9, 0.5$ and 0.1. The curve for $\delta = 0.9$ in particular is seen to be severely distorted by the 'fluctuation

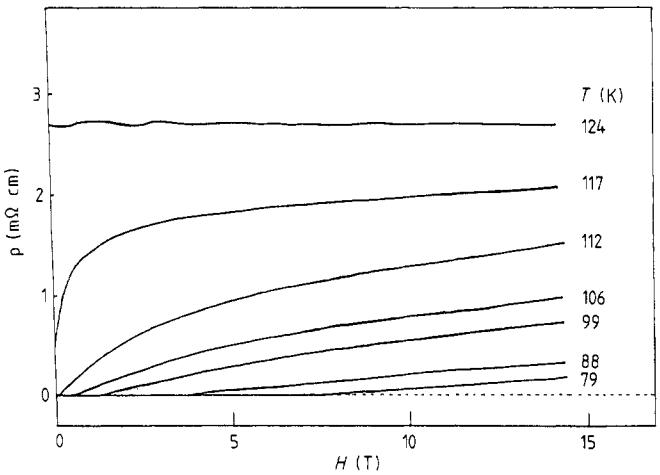

Figure 7. Resistivity against field at fixed T.

effects.' The dotted curves in figure 6 show the level curves for an alternative representation of ρ_n. This is found by fitting a simple Taylor series to ρ only in the range below 130 K. With the restriction that $\rho_n(T = 0) \geqslant 0$, a solution of the form of equation (5) could not be found, the simplest solution being

$$\rho = B_1 T + B_2 T^4 \tag{6}$$

where $B_1 = 9.44\ \mu\Omega\ \text{cm K}^{-1}$, $B_2 = 6.6 \times 10^{-3}\ \text{n}\Omega\ \text{cm K}^{-4}$. The dotted curves in figure 6 represent equation (6) for $\delta = 1.0, 0.9, 0.5$ and 0.1. The dotted and broken level curves run approximately parallel to each other, differing primarily in the precise value of δ; they are also not very different from the horizontal lines which Tinkham [5] used in his analysis. This is fortunate, since a proper incorporation of fluctuation effects is beyond the scope of this paper. In summary, it can be seen that the *scaling* behaviour (H against T for the level curves) is insensitive to the choice of ρ_n; on the other hand, values of δ extracted from the experimental data (or, equivalently, of H_0, defined below in equation (11)) are subject to substantial error. The scaling curves $H_n(T)$ (extracted from the dotted curves of figure 6 for $\delta = n/10$) are plotted in figure 8 and compared with the theoretical form discussed below.

Three other sets of data are also plotted in figure 8. Two sets are values of H^*_{c2}, one for the unoriented pellets and the other for the $H \parallel (a, b)$ grains in epoxy. The differences between the two curves are relatively small. The third set is an estimate of H^T_{c2}, the threshold field at which resistance first appears. This is a subjective criterion, subject to large uncertainty since it corresponds to a very small resistance, $\delta \leqslant 10^{-2}$. Indeed, the theory shows that there is not a well defined threshold, but only an exponentially decreasing ρ as T decreases. It is included here mainly to show that there is a substantial inequality,

$$H^*_{c2} < H^T_{c2}. \tag{7}$$

This inequality is expected theoretically [5, 6]. In a fluid regime, there will still be an apparent $j_c = 0$ at low temperatures or low fields, simply because the rate of thermal activation becomes so low that equilibrium is not achieved in the finite duration of the experiment. Theoretical estimates suggest that H^*_{c2}, in the fluid regime, is approximately

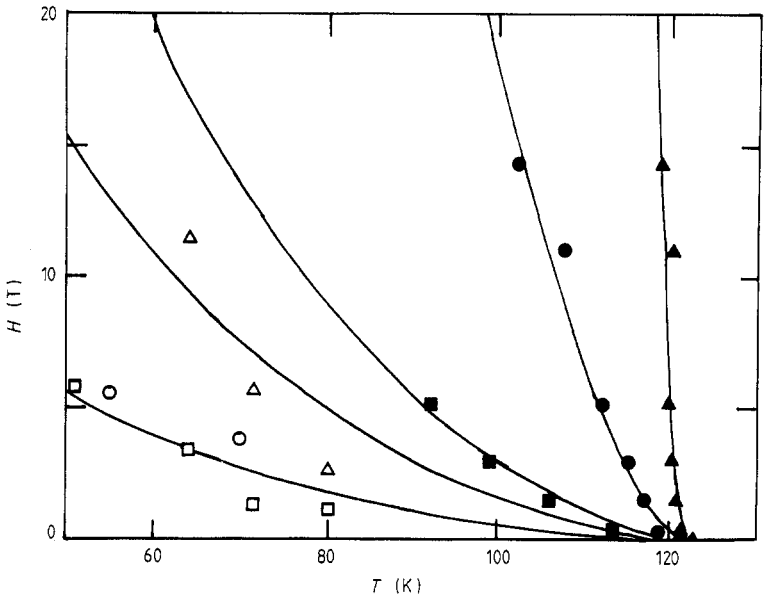

Figure 8. Scaling fields against T: H_9 (▲), H_5 (●), H_1 (■), H_{c2}^{T} (△) and H_{c2}^{*} both for pellets (□) and oriented grains (○ = $H\| \pm a, b$). Full curves are given by equation (11), for various values of H_0.

a level curve corresponding to $\delta \sim 10^{-7}$. We shall see that this behaviour is largely in agreement with experiment.

The inequality (equation (7)) is not found in transport measurements of j_c on thin films. However, this is expected whenever j_c is measured by direct transport techniques. In fact, it is a tautology: $j_c = 0$ is equivalent to $R \equiv \lim_{I \to 0}(V/I) = 0$.

4. Discussion

4.1. Flux creep

There is a close relationship between the experimental fields H_{c2}^{*} and the $H(T^*)$ introduced by Müller *et al* [11] (MTB). In appendix 2 it is shown that within the critical-state model they are identical. Hence the discussions of references [5] and [6] should apply to H_{c2}^{*}. YM [6] shows that $H(T^*)$ could be interpreted in terms of flux creep: thermally activated depinning of vortex lines from pinning centres. Tinkham [5] showed that the broadening of the resistive transition can be described by Ambegaokar–Halperin theory [12].

$$\rho/\rho_n = [I_0(U_P/2k_B T)]^{-2} \tag{8}$$

where U_P is the pinning energy of a vortex and I_0 is a modified Bessel function. Tinkham writes

$$U_P = (3\sqrt{3}\Phi_0^2\beta/2c)J_c/H \tag{9}$$

where $\beta \simeq 1$ is a numerical constant and J_c is the intrinsic Ginzberg–Landau critical current density which is proportional to $(1 - t)^{3/2}$ near T_c where $t = T/T_c$. Equations (8)

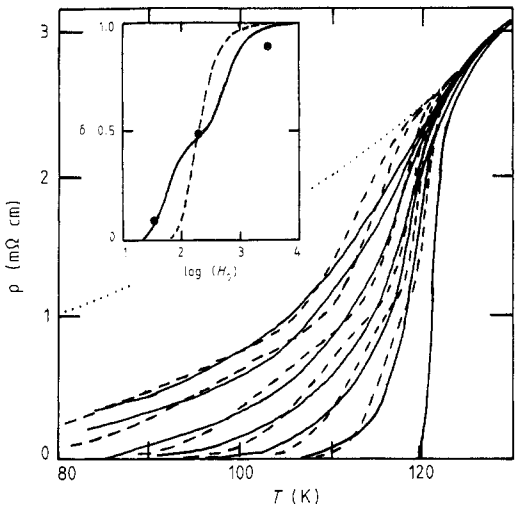

Figure 9. Resistivity against T at various fields: same data as figure 6, but now including the fits to anisotropic flux-creep theory (i.e., inserting equation (12) into equation (8)). Full curves are the data; broken curves are the theory; dotted curve is the normal-state resistance (equation (6)). Inset: full circles are the values of H_0 (equation (10)) obtained from fitting H_0, H_5 and $H_1(T)$, figure 8. The broken curve is the best fit to equation (8) assuming isotropioc resistivity; the full curve includes the resistivity anisotropy (equation (12)).

and (9) may be recast to say that the level curves of ρ (i.e. $\rho/\rho_n = \delta$) are all related by a scaling relation

$$H = H_0(\delta)g(t) \tag{10}$$

where

$$g(t) = (1 - t^2)(1 - t^4)^{1/2}/t \tag{11a}$$

$$\xrightarrow[t\to 1]{} 4(1 - t)^{3/2}. \tag{11b}$$

The full curves in figure 8 show that equation (10) is well satisfied for $\delta = 0.9$, 0.5 and 0.1. Moreover, within the flux-creep regime $j_c = 0$, and an apparent non-zero j_c appears only as a result of slow thermal depinning. YM show that the experimental duration can be related to a particular value of $\delta \sim 10^{-7}$. Hence H^*_{c2} should also scale according to equation (10). This is seen to be the case in figure 8.

However, the values of $H_0(\delta)$ are in poor agreement with theory (broken curve in the inset to figure 9). This is in stark contrast to the excellent agreement found by Tinkham [5] in analysing single-crystal [13] and epitaxial-film [14] data. Taken together with the good scaling (figure 8), this strongly suggests that the lack of agreement is due to neglect of anisotropy in the polycrystalline data. In § 4.2 it is suggested that anisotropy may be approximately accounted for by replacing ρ in equation (8) by

$$\bar{\rho} = (\rho_\parallel + \rho_\perp)/2. \tag{12}$$

Here, $\rho_\parallel(\rho_\perp)$ is found from equations (8) and (9) by substituting $J_c \to J_{c\parallel}(J_{c\perp})$, where $J_{c\parallel}/J_{c\perp} = \xi_\perp/\xi_\parallel = H_{c2\parallel}/H_{c2\perp} = 10$. This leads to good agreement with experiment both for $\rho(T)$ and $H_0(\delta)$ (figure 9). From these fits, we find $\beta J_{c\parallel}(T = 0) = 5.3 \times 10^6$ A cm^{-2}, compared with 1.8–4 $\times 10^7$ cm^{-2} for YBCO [5]. Moreover, within this model H^T_{c2} corresponds to $\delta = 1.5 \times 10^{-2}$ and H^*_{c2} to $\delta = 5 \times 10^{-6}$. As anticipated, H^T_{c2} does not follow a scaling relation very accurately, but these values of δ are in good agreement with expectation.

4.2. Anisotropy

Analysis of the pressed pellet data is complicated by the strong two-dimensional anisotropy of these materials, $\rho_c/\rho_a > 100$, or $H_{c2\parallel}/H_{c2\perp} \geqslant 10$. In effective-medium theory, it can be shown [15] that for randomly oriented grains the $\rho_c \to \infty$ limit can be taken, and the equivalent resistivity is just twice that of a two-dimensional medium, with neglect of the grains aligned along ρ_c. In a field, the grains will still have a random distribution of the angle between the applied field and the conductivity plane, and since $H_{c2\parallel} \neq H_{c2\perp}$, this will lead to a broadening of the resistive transition. Ths broadening will occur even in the absence of flux-creep broadening. In reference [15] an attempt was made to interpret the broadening in $YBa_2Cu_3O_{7-\delta}$ solely in terms of H_{c2} anisotropy. This interpretation can be shown to be incorrect for the following reasons: (i) the broadening is present in single crystals; (ii) the analysis of reference [15] overestimates the H_{c2} anisotropy; (iii) in the present samples, we have found that the anisotropy broadening predicted by reference [15] is too small, even in the limit $H_{c2\perp} \to 0$, to explain the data. Hence the primary cause of the broadening must be the flux-flow mechanism. Nevertheless, there remains the problem of incorporating the anisotropy into the flux-flow analysis.

In effective-medium theory, the distribution of grains in a field is approximately equivalent to a bimodal distribution, with half of the grains having field parallel to the *a–b* plane, with $\rho = \rho_\parallel$, and half with $\rho = \rho_\perp$. Then $\rho_{\text{eff}} = \sqrt{\rho_\parallel \rho_\perp}$, since the system is at the percolation limit. Incorporation of this limit into the flux-flow theory yields level curves almost equivalent to the isotropic case—and hence poor agreement between experiment and theory. We have empirically found that the arithmetic mean (equation (12)) provides a satisfactory description of our data for a ratio $H_{c2\parallel}/H_{c2\perp} = 10$, as discussed in § 4.1. Figure 9 compares the experimental $R(H, T)$ curves (full curves) with the theoretical values found by using equation (8) to calculate $\bar{\rho}$ (broken curves). Close inspection of figure 9 reveals that the agreement is only approximate: the experimental data resemble a smoothed-out version of the theory, with no evidence of the predicted fine structure. This is to be expected, since a proper theory would average the resistivity over all possible orientations of the field with respect to the crystal axes.

The form of equation (8) is suggestive of a series combination of resistors. It has recently been pointed out [16] that the normal-state resistivity of the high-T_c superconductors displays giant deviations from Matthiessen's rule. This can be understood if most grain boundaries are opaque to electronic transport, leaving only a few convoluted paths through the material. In this case, it is clear that the number of parallel channels is limited, so ρ will be a series average (equation (12)) over the differently oriented grains.

4.3. Flux-lattice melting

Figure 10 shows the data on H^*_{c2} extended to lower temperatures. (The other fields in figure 8 cannot be measured at these temperatures in the available field range $H \leqslant 15$ T.) Also shown is the extrapolation of the scaling curve of figure 8 (dotted curve). A clear break is observed near $T = 40$ K, the experimental H^*_{c2} values falling significantly above this curve at lower temperatures. This can be understood in terms of flux-lattice melting [17, 18] as discussed in a recent paper [19]. In order to compare the experimental melting curve with theory, the critical field $H_{c2\parallel}$ must be known. This is estimated as follows. Werthamer–Helfand–Hohenberg [20] theory is used to determine $H_{c2}(T)$ in terms of

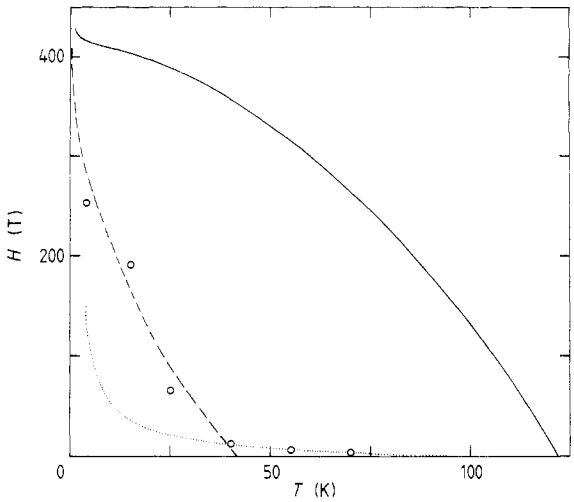

Figure 10. Critical fields against T. Open circles are $H^*_{c2\|}$; full curve is $H_{c2\|}$; broken curve is H_M; dotted curve is flux-flow scaling, equation (11) (similar to figure 8, but adjusted for best fit of $H^*_{c2\|}$ data). See discussion in text.

two parameters, $H_{c2}(0)$ and λ_{so}, the spin–orbit scattering parameter. Essentially, λ_{so} is adjusted to describe H_{c2} near T_c, while $H_{c2}(0)$ is adjusted to give the best agreement between H^*_{c2} and the melting curve, $H_M(T)$. There is some uncertainty in determining $H_{c2}(T \simeq T_c)$, since the above calculations (figure 8) implicitly assumed that T_c is independent of H. Rather arbitrarily, the field H_9 has been equated with H_{c2}. For the present purposes the error is likely to be small, since H_9 varies from zero to 15 T as T changes by only 3 K, while the melting is only sensitive to $T < 40$ K. The value $\lambda_{so} = 10$ may be taken as representative, with large error bars. With this value, $H_{c2}(0) \simeq 430$ T, and the full curve of $H_{c2}(T)$ is shown in figure 10. The melting curve extrapolates to $T_M = 40$ K at $H = 0$. This value is in good agreement with that of Gammel *et al* [21], who find $T_M = 40$ K in a $T_c = 110$ K Tl compound and $T_M = 30$ K in a Bi compound.

Given the critical field, the melting curve H_M can be constructed if a melting parameter, γ_M, is known where

$$\gamma_M = \gamma_M^0/\sqrt{1-\delta_M} \tag{13a}$$

$$\gamma_M^{02} = 2(4\pi)^3\sqrt{3}\lambda_0^2 k_B T_c/\alpha\phi_0^2 \tag{13b}$$

$$\delta_M = \pi\, e(n_p/d)^{1/2} f_p/C_{66}. \tag{13c}$$

Here λ_0 is the London penetration depth at $T = 0$, d is the grain diameter, α is a numerical coefficient $\simeq 1$, n_p the density of pins, f_p the force per pin and C_{66} the flux lattice shear modulus and e the base of natural logarithms. The factor δ_M is an approximate correction factor to allow for pinning effects [18, 22, 23]. The broken curve in figure 10 corresponds to $\gamma_M = 1.7$. The value is about an order of magnitude larger than the value of γ_M^0 inferred from equation (13*b*). While the correction factor δ_M renormalises γ_M^0 in the right direction, the large magnitude of the renormalisation suggests that a more accurate theory of pinning effects may be needed.

Because of the bend rigidity, the flux lattice can be treated as two-dimensional. However, when it disorders the correlation length parallel to the field collapses, so the

fluid and glassy phase must be treated as three-dimensional. Nelson [24] has suggested that there could be unusual vortex entanglement effects in this fluid phase. Since H_M is proportional to H_{c2}, the melting should also be anisotropic, occurring first when the field lies along the crystalline c axis. This may be the origin of the deviations from scaling observed in figure 5(b) [25].

Note added in proof. The unexpectedly small bend modulus of the vortex lattice necessitates a three-dimensional treatment of flux-lattice melting. A Lindemann criterion approach yields good agreement with the data [30].

4.4. Flux-lattice phase diagram: solid, liquid, glass

MTB [11] pointed out that the scaling relation, equation (11b), has the same exponent as the deAlmeida–Thouless (AT) line [26] in a spin glass. They suggested that this resemblance was not accidental, and that the high-T_c superconductors are examples of a glassy superconductor—an array of Josephson-coupled superconducting 'grains' [27]. It soon became clear that the 'grains' must be considerably smaller than the actual physical grains making up the ceramic superconductors, and YM suggested an alternative derivation of equation (12b) in terms of flux creep (discussed above). Tinkham [5] suggested that the distinction between glassy superconductivity and the flux-creep regime is largely semantic. In high fields, the 'grains' must be coherent superconducting regions considerably smaller than the physical grains; Tinkham associates them with coherent regions of a flux lattice. The Josephson energy of a grain in one picture is equated with the pinning energy in the other; more precisely, $2E_J = U_p$.

The present results support Tinkham's viewpoint, with one subtle difference. The scaling is observed at temperatures above the temperatures at which the flux lattice has melted. Hence, it may be interpreted as a classical glass transition, from fluid to disordered glass, within the flux vortex fluid. In the presence of weak pinning, the flux lattice locally distorts to accommodate the pin distribution, with strains being relieved by grain-boundary formation. As the number or strength of the pins increases, more grain boundary is formed until, beyond a critical pinning strength, the grain size collapses to ~zero, leading to a disordered state (glass). The distinction between glass and fluid depends on whether vortices can flow in response to an applied current. As such $H^*_{c2}(T)$ does not appear to be a thermodynamic phase boundary, but depends on the effective observation time. This same holds true for an ordinary glass transition and, apparently, the spin–glass AT line as well. This interpretation provides a satisfying picture of a glassy superconductor.

It is not immediately apparent that Tinkham's analysis is restricted to a fluid or strongly disordered phase. We believe that this arises in equation (10), from treating β as a field-independent constant. This parameter is proportioned to the ratio $\Delta U/2E_J$, where E_J is the average vortex energy and ΔU the average change in energy per vortex due to pinning. If the number of pinning centres per unit volume n_p is low compared with the flux density n, then

$$\Delta U/2E_J \propto n_p a/n \tag{14}$$

where a is a vortex lattice constant, $n = B/\phi_0 = 2/(\sqrt{3}a^2)$, where $\phi_0 = hc/2e$ is the superconducting flux quantum. In this case, $\beta \sim H^{-3/2}$, in contrast to Tinkham's assumption that β is constant. Hence Tinkham's model only holds in the strong-disorder limit, with many more pinning centres than flux lines.

The above results somewhat moderate the pessimistic opinions expressed in reference [5]. The very low intragrain j_cs seem to be associated with the fluid vortex phase. Since $H_M \propto H_{c2}$, discovery of superconductors with higher T_c (and hence higher H_{c2}) should allow a vortex lattice to persist to higher temperatures. Horeover, since γ_M depends on pinning, it may prove possible to enhance H_M even in the presently known compounds.

5. Conclusions

We have shown that flux-creep theory provides an excellent description of the broadening of the resistive transition in $TlBa_2Ca_3Cu_4O_x$, when proper account is taken of anisotropy effects. The same theory also properly describes the temperature dependence of the scaling field, H_{c2}, at higher temperatures, although a sharp rise in H^*_{c2} below 40 K may signal the flux-lattice melting transition. Recently, Hettinger *et al* [2] provided additional evidence in favour of a flux-creep theory, by showing that the theory does predict a scaling of j_c against H, T which is very similar to the Kramer form, equation (1).

Acknowledgments

These experiments were carried out at the Francis Bitter National Magnet Lab, which is supported at MIT by the NSF. This research is supported in part by a grant from E I DuPont de Nemours and Company (RSM, KC, BM), and in part by NSF Grant No DMR-85-13626 (AKS, JSB). Early stages of the work were sponsored by the US–Israel Binational Science Foundation (RSM, KC, BM). We wish to thank D R Nelson and J V Jose for interesting conversations, and P Haldar and B C Giesen for providing us with the samples.

Appendix 1. Orienting *P*-factor

To quantify the degree of *c*-axis alignment, we have introduced a convenient measure, the *P*-factor, based on relative x-ray intensities. In a perfectly aligned sample, only (00*l*) reflections would contribute to x-ray reflection from the sample *c* face. Hence a measure of orientation is

$$P = (1 - \Gamma) \times 100\% \tag{A.1}$$

where Γ is the relative intensity of the strongest forbidden (non-(00*l*)) reflection, normalised to an unoriented sample. Specifically, $\Gamma = (I_{hkl}/I_{00l})^{o}/(I_{hkl}/I_{00l})^{u}$, where I_{hkl} stands for the intensity of the *hkl* x-ray reflection intensity, the subscript *hkl*(00*l*) refers to a particular forbidden (allowed) reflection, and the superscript o(u) means that the measurement is carried out on an (un)oriented sample.

This measure can be related to a more familiar measure as follows. If the oriented sample is characterised by a gaussian spread of *c* axes of width θ_0, then

$$\Gamma = \sum_i f_i \exp[-(\theta_i/\theta_0)^2]. \tag{A.2}$$

Here it is assumed that the forbidden reflection is degenerate, with the *i*th reflection

having a relative contribution f_i, and θ_i is the angle between the reflecting normal and the c axis, $\cos\theta_i = l/\sqrt{h^2 + k^2 + l^2}$. For instance, in $YBa_2Cu_3O_7$, we have oriented samples with $P = 98\%$, based on the (approximately) degenerate reflections (110), (103) and (013). For these reflections $f_1 \simeq f_2 \simeq f_3 = 1/3$ (from model calculations), $\theta_1 = 90°$ and $\theta_2 = \theta_3 = 18.4°$. Thus $P = 98\%$ corresponds to $\theta_0 = 9.8°$, still a substantial spread. (Note that the contribution of θ_1 to Γ is negligible.) This result is in accord with rocking-angle x-ray measurements on similarly prepared samples [28].

For $TlBa_2Ca_3Cu_4O_x$, the reflection corresponding to (200) and (117) is used. Here the f_i are more sensitive to the model parameters but approximately $f_1 = 0.59, f_2 = 0.41$, $\theta_1 = 90°$ and $\theta_2 = 11.42°$. Hence $P = 98\%$ implies $\theta_0 \simeq 10.0°$.

Armed with this information, we can ask whether the anomalous behaviour of figure 5(b) could be explained by a certain fraction of misaligned grains. In the related Bi compounds, $H_{c2}(\theta) \simeq H_{c2\perp}$ unless θ is within 10° of the parallel axis [29]. (Actually, the quantity measured is the H_{c2}^{T} anisotropy.) This feature has to do with the strong two-dimensional anisotropy, and is likely to be similar to Tl compounds. Hence, the parallel-field behaviour will only arise in those grains which are misaligned by at least 80°. The probability for the misalignment angle θ to be greater than 80° is $\leqslant \exp[-(80/10)^2] \simeq 10^{-28}$, i.e. totally negligible.

Appendix 2. $H_{c2}^{*} = H(T^{*})$

Within the critical-state model [9], the hysteretic magnetisation of a superconducting grain has a unique upper bond, $\Delta M/2$, corresponding to the maximum critical current j_c circulating in the same direction throughout the grain. There is likewise a unique lower bound, $-\Delta M/2$, corresponding to the same current circulating in the opposite sense. In a zero-field-cooled (ZFC) experiment [11], the measured (hysteretic) magnetisation corresponds to maximal flux exclusion at that field and temperature, or $M_{ZFC} = -\Delta M/2$. In a field-cooled (FC) measurement, M_{FC} corresponds to maximum flux trapping, or $M_{FC} = \Delta M/2$. Hence, $M_{FC} - M_{ZFC} = \Delta M$; thus both quantities vanish at the same field, or

$$H(T^{*}) = H_{c2}^{*}. \tag{A.3}$$

The adequacy of the critical-state model can be tested by studying minor hysteresis loops. With the critical-state model, the magnetisation should switch from $\Delta M/2$ to $-\Delta M/2$, when the applied field decreases by $\Delta H = 4\pi\Delta M$. This is approximately satisfied (to ~10% at low T; to a factor of two near H_{c2}^{*}; see figure 3) by our data. The critical-state model must break down at very low fields where intergrain currents becomes significant, but equation (A.3) should hold for the present experiments.

References

[1] Bednorz J G and Müller K A 1986 *Z. Phys.* B **64** 189
[2] Satchell J S, Humphreys R G, Chew N G, Edwards J A and Kane M J 1988 *Nature* **334** 331
Hettinger J D, Swanson A G, Skocpol W J, Brooks J S, Graybeal J M, Mankiewich P M, Howard R E, Straughn B L and Burkhardt E G 1989 *Phys. Rev. Lett.* **62** 2044
[3] Chen K, Maheswaran B, Haldar P, Markiewicz R S and Giessen B C 1989 *J. Appl. Phys.* **65** 3574
[4] Kramer E J 1973 *J. Appl. Phys.* **44** 1360
[5] Tinkham M 1988 *Phys. Rev. Lett.* **61** 1658

[6] Yeshurun Y and Malozemoff A P 1988 *Phys. Rev. Lett.* **60** 2202
[7] Haldar P, Chen K, Maheswaran B, Roig-Janicki A, Jaggi N K, Markiewicz R S and Giessen B C 1988 *Science* **241** 1198
[8] Farrell D E, Chandrasekhar B S, DeGuire M R, Fang M M, Kogan V G, Clem J R and Finnemore D K 1987 *Phys. Rev.* B **36** 4025
[9] Bean C P 1964 *Rev. Mod. Phys.* **36** 31
[10] Swanson A *et al* unpublished
[11] Müller K A, Takashige M and Bednorz J G 1987 *Phys. Rev. Lett.* **58** 1143
[12] Ambegaokar V and Halperin B I 1969 *Phys. Rev. Lett.* **22** 1364
[13] Iye Y, Tamagai T, Takeya H and Takei H 1988 *Superconducting Materials* ed. S Nakajima and H Fukuyama *Japan. J. Appl. Phys. Ser. 1* p 46
[14] Oh B, Char K, Kent A D, Naito M, Beasley M R, Geballe T H, Hammond R H and Kapitulnik A 1988 *Phys. Rev.* B **37** 7861
[15] Markiewicz R S, Chen K and Jaggi N K 1988 *Phys. Rev.* B **37** 9336
[16] Markiewicz R S 1988 *Solid State Commun.* **67** 1175
[17] Huberman B A and Doniach S 1979 *Phys. Rev. Lett.* **43** 950
[18] Fisher D S 1980 *Phys. Rev.* B **22** 1190
[19] Markiewicz R S 1988 *J. Phys. C: Solid State Phys.* **21** L1173
[20] Werthamer N R, Helfand E and Hohenberg P C 1966 *Phys. Rev.* **147** 295
[21] Gammel P L, Schneemeyer L F, Waszczak J V and Bishop D J 1988 *Phys. Rev. Lett.* **61** 1666
[22] Larkin A I and Ovchinnokov Yu N 1979 *J. Low Temp. Phys.* **34** 409
[23] Mullock S J and Evetts J E 1985 *J. Appl. Phys.* **57** 2588
[24] Nelson D R 1988 *Phys. Rev. Lett.* **60** 1973
[25] Markeiwicz R S unpublished
[26] de Almeida J R L and Thouless D J 1978 *J. Phys. A: Math. Gen. Phys.* **11** 983
[27] Ebner C and Stroud A 1985 *Phys. Rev.* B **31** 165
[28] Hart Jr H R private communication
[29] Naughton M J, Yu R C, Davies P K, Fischer J E, Chamberlin R V, Wang Z Z, Jing T W, Ong N P and Chaikin P M unpublished
[30] Markiewicz R S 1989 *J. Phys.: Condens. Matter* at press